PROCEEDINGS REPRINT

SPIE–The International Society for Optical Engineering

Reprinted from

Laser Applications in Combustion and Combustion Diagnostics II

25–26 January 1994
Los Angeles, California

Volume 2122

Resonance lamp absorption technique for simultaneous determination of the OH concentration and temperature at 10 spatial positions in combustion environments

B. Shirinzadeh and Ray W. Gregory
NASA Langley Research Center
Hampton, VA 23681

ABSTRACT

A rugged, easy to implement, line-of-sight absorption instrument which utilizes a low pressure water vapor microwave discharge cell as the light source, has been developed to make simultaneous measurements of the OH concentration and temperature at 10 spatial positions. The design, theory, and capability of the instrument are discussed. Results of the measurements obtained on a methane/air flat flame burner are compared with those obtained using a single-frequency, tunable dye laser system.

1. INTRODUCTION

The hydroxyl radical (OH) is a chemical intermediate produced during most combustion processes. Its properties have been studied for many years and there exits a vast number of publications and data on its rotational electronic structure. This information has allowed it to be used as a tool for nonintrusive diagnostics of combustion environments. One important application in aeronautics is the determination of the static temperature in scramjet engines. Various laser-based techniques such as degenerate four-wave mixing (DFWM),[1,2] laser-induced fluorescence (LIF),[3,4] and line-of-sight absorption measurements[5,6] have been used to determine the temperature and OH concentration in flames. All of the above laser-based techniques require expert people with extensive experience in laser techniques and electronics to obtain meaningful data. Some years ago, a single-position OH system based on a microwave resonance lamp absorption technique was developed by our group at NASA Langley Research Center.[7] The purpose of this system was to monitor the static temperature in supersonic combustors on a routine basis. Such environments are noisy, lack easy optical access, and are extremely harsh for laser-based diagnostics. After the single-position OH instrument was successfully demonstrated in a Mach 2 combustor,[8] the need for a multi-position OH instrument was identified. In this paper, the design, the theory, and the calibration of a 10-position OH temperature and density monitoring system will be presented. In addition, experimental results that were obtained on a methane-air flat flame burner using this instrument will be discussed. A comparison of these results with those obtained using a single-frequency tunable dye laser system will demonstrate the capability and accuracy of this instrument.

2. THEORY

2.1. Evaluation of the transmitted intensities

The 10-position OH instrument is an extension of the single-position OH instrument which was developed by our group some years ago at NASA Langley Research Center. It utilizes the line-of-sight absorption technique to measure simultaneously not only the effective product of the OH concentration times the path length but also the effective rotational temperature of OH along the absorption path at ten spatial positions. It uses a low pressure (1 Torr) water-vapor microwave discharge cell as the light source. The OH emission spectrum in the rotational electronic

0-8194-1415-8/94/$6.00

transitions[9] from $^2\Sigma^+(v' = 0)$ to $^2\Pi(v'' = 0)$ and from $^2\Sigma^+(v' = 1)$ to $^2\Pi(v'' = 1)$ after traversing a sample volume (i. e. a flame) is dispersed using a spectrograph. On the exit plane of the spectrograph, a series of fiber arrays are installed such that each fiber array collects a specified portion of the transmitted OH spectrum. There exists eight spectral channels at the exit plane of the monochromator. Comparison of the signal detected in each fiber array between the flame on and off conditions, yields the fraction of the light that is transmitted for each spectral channel. It can be shown that this fraction is given by

$$Tau_i = \frac{\int_{\nu_1}^{\nu_2} T_i(\nu).\, I(\nu).\, d\nu}{\int_{\nu_1}^{\nu_2} T_i(\nu).\, I_o(\nu).\, d\nu} \qquad (1)$$

where $T_i(\nu)$ is the frequency dependent transmission profile of the ith spectral channel, $I(\nu)$ and $I_o(\nu)$ are respectively the frequency dependent transmitted and emission intensities of OH, and ν_1 and ν_2 are the limits of integration over the frequency for which $T_i(\nu)$ differs from zero.

The emission (lamp) intensity $I_o(\nu)$ is the convolution of a series of rotational electronic lines of OH which lie in the frequency range from ν_1 to ν_2. The relative peak intensities, I_{oj}, of the OH emission lines from the microwave discharge cell have been measured using a single 2 meters monochromator at various microwave discharge powers ranging from 50 to 100 watts. The emission line shape for a given rotational electronic transition of OH is given by a Doppler profile. The translational temperature of OH in the discharge was deduced from the observed linewidth which was measured using an absorption technique that utilizes the intensity-stabilized output of a frequency-doubled, single-frequency tunable ring dye laser. For the jth rotational electronic transition of OH the emission profile can be expressed as

$$I_{oj}(\nu) = I_{oj} \exp[-(\nu - \nu_j)^2/(\Delta_o)^2] \qquad (2)$$

I_{oj} is the peak intensity of the jth rotational electronic line having a transition frequency of ν_j. Δ_o is the Doppler broadening parameter which is related to the Doppler full width at half maximum $\Delta\nu_{oD}$ by

$$\Delta_o = \Delta\nu_{oD}/[2\,(\mathrm{Ln}\ 2)^{1/2}] \qquad (3)$$

$\Delta\nu_{oD}$ is given by

$$\Delta\nu_{oD} = 17.368 \times 10^{-8}\, \nu_j\, (T_e)^{1/2} \qquad (4)$$

where T_e is the translational temperature of OH molecules in the microwave discharge cell. To minimize the amount of computations, only those OH lines whose frequency, ν_j, lie in the range from $(\nu_D - 4\,\Delta\nu_D)$ to $(\nu_D + 4\,\Delta\nu_D)$, where $\Delta\nu_D$ is the Doppler linewidth of the absorption transition, are considered in the convolution. If the range of j for these transitions are denoted from k to l then the expression for $I_o(\nu)$ is given by

$$I_o(\nu) = \sum_{j=\kappa}^{l} I_{oj}(\nu) \qquad (5)$$

The transmitted intensity of the light $I(\nu)$ through a column of OH with an effective path length L and an effective concentration [OH] is given by

$$I(\nu) = I_o(\nu).\, \exp\left(-\sum_{j=\kappa}^{l} n_j.\, \sigma_j(\nu).\, L\right) \qquad (6)$$

where $I_o(\nu)$ is defined by equation (5), n_j is the density of OH molecules in the rotational level from which the jth absorption transition originates, and $\sigma_j(\nu)$ is the absorption cross section for the jth rotational electronic transition. Like before, the summation is over rotational electronic transitions which satisfy the condition for Eq. (5).

The density of OH molecules in a given rotational level K" in the ground electronic state is given by

$$n_j = [OH].\, \Delta n/n \qquad (7)$$

where the fractional population $\Delta n/n$ is expressed by the Boltzmann equation

$$\Delta n/n = Z^{-1}\, (2J" + 1)\, \exp[-E_{J"}/(k_B T)] \qquad (8)$$

where J" can assume values of $J" = K" \pm 1/2$, $E_{J"}$ is the energy of the rotational level, k_B is the Boltzmann constant, and T is the temperature. (Here it is assumed that the molecule is in thermal equilibrium.) Finally, Z is the partition function given by

$$Z = \sum_{J"} (2J" + 1)\, \exp[-E_{J"}/(k_B T)] \qquad (9)$$

Here the sum is over all the rotational levels in v" = 0, 1, 2, and 3 in the ground electronic state, and the splitting of the levels due to Λ-doubling has been taken into account

The absorption cross section, $\sigma_j(\nu)$, can be expressed as

$$\sigma_j(\nu) = \sigma_{oj}\, g_j(\nu) \tag{10}$$

where $g_j(\nu)$ is the normalized line shape function satisfying the equation

$$\int_{-\infty}^{\infty} g_j(\nu)\delta\nu = 1 \tag{11}$$

, and σ_{oj} is the integrated absorption cross section for the jth rotational electronic transition defined by

$$\sigma_{oj} = \pi\, r_o\, f_{v"v'}\, (\Delta f/f)_j \tag{12}$$

where $r_o = e^2/(mc^2) = 2.818 \times 10^{-13}$ cm is the classical radius of the electron, $f_{v"v}$ is the band oscillator strength in absorption (for a rotationless molecule $f_{oo} = 1.09 \times 10^{-3}$ and $f_{11} = 0.69 \times 10^{-3}$),[10] and $(\Delta f/f)j$ is the fractional band oscillator strength for the absorption line. The subscripts v" and v' denote the vibrational manifolds in the ground and excited electronic states, respectively.

The normalized absorption line shape function $g_j(\nu)$ is expressed as[11]

$$g_j(\nu) = H(x, a, b, c)/[\Delta(\pi)^{1/2}] \tag{13}$$

where Δ is the Doppler broadening parameter defined by Eq. (3) with a temperature T instead of T_e in Eq. (4), and H(x, a, b, c) is the hard collisional narrowing profile and is expressed as

$$H(x, a, b, c) = \mathrm{Re}\{W(z)/[1-(\pi)^{1/2}bW(z)]\} \tag{14}$$

where

$$x = (\nu - \nu_j)/\Delta,\ a = \gamma_j/\Delta,\ b = \alpha_j/(2\,\pi\,\Delta),\ c = \beta/\Delta \tag{15}$$

and

$$W(z) = i/\pi \int_{-\infty}^{\infty} dy\, \exp(-y^2)/(y - z),\ z = (x - c) + i(a + b) \tag{16}$$

with collision induced broadening, narrowing, and shift parameters respectively defined as γ_j, α_j, and β. The complex error function, W(z), is computed using an algorithm described by Hui et. al.[12] with a sixth order polynomial.

To compute the collision induced shift and broadening parameters β and γ_j, the impact approximation is used.[13] Within the frame work of this approximation, the broadening parameter (half of the full width at half maximum) is given by

$$\gamma = 2\pi n' v_r \int_0^{\infty} d\rho.\rho \{1 - \cos \eta(\rho)\} \tag{17}$$

and the collision-induced shift in the line center is expressed as

$$\beta = 2\pi n' v_r \int_0^{\infty} d\rho.\rho \sin \eta(\rho) \tag{18}$$

where n' is the density of the buffer gas, v_r is the relative speed between the colliding partners, ρ is the impact parameter, and $\eta(\rho)$ is the phase shift described by

$$\eta(\rho) = \int_{-\infty}^{\infty} U(R)\, dt,\ R = [v_r^2 t^2 + \rho^2]^{1/2} \tag{19}$$

where U(R) is the interaction potential between the colliding partners: for van der Waals (induced dipole-dipole) interaction $U(R) = C_6/R^6$, for resonance (dipole-dipole) interaction $U(R) = C_3/R^3$, and for Lennard-Jones potential $U(R) = C_{12}/R^{12} - C_6/R^6$. C_3, C_6, and C_{12} are the interaction constants.

To compute the collision induced broadening parameter, it is noted that in a hydrocarbon/air or hydrogen/air combustion process there exits H_2O, N_2, O_2, CO_2 and H_2 molecules. It has also been shown that OH broadening due to water molecules is J-dependent because of the near-resonance interaction between the two species.[14,15] The broadening parameter in this case is represented by γ_R (resonant). There is no significant J-dependence for the other gases mentioned above, and those collisions are represented by γ_{NR} (non-resonant).

For nonresonance interaction of OH with buffer gas molecules, it may be argued that the broadening is mostly due to collisions involving small impact parameter, while the shift is due to those collisions with large impact parameter. This implies that, for the Lennard-Jones potential, the collision-induced broadening is due primarily to the C_{12}/R^{12} term, and the collision-induced shift is due primarily to the $-C_6/R^6$ term. Assuming a $U(R) = C_{12}/R^{12}$ and using Eqs. (17) and (19), a temperature dependence of $T^{-0.59}$ is obtained for the broadening. For $U(R) = -C_6/R^6$ and using Eqs. (18) and (19), a temperature dependence of $T^{-0.7}$ is obtained for the shift. Collision-induced shift and broadening of OH by molecular oxygen and nitrogen have been measured at room temperature ($2\gamma = (18.8 \pm 0.7) \times 10^{-5}$ cm^{-1} Torr^{-1} for O_2 and $2\gamma = (28.5 \pm 0.7) \times 10^{-5}$

cm^{-1} $Torr^{-1}$ for N_2).[16] CO_2 and N_2 molecules have comparable size, again based on the above argument (the broadening is due to collisions with small impact parameter, $R = a_{OH} + a_{buffer}$, where a is the radius of the molecule), the broadening of OH due to CO_2 molecule should be about the same as that of N_2 molecule. Results obtained by R. Engleman, Jr.[17] indicate a value of $2\gamma = 20.7 \times 10^{-5}$ cm^{-1} $Torr^{-1}$ for the OH broadening by the CO_2 molecule at room temperature. This value however is on the low side, when extrapolated to high temperatures and compared with the results obtained by Rea et. al.[15] For this computation the collision-induced broadening of OH by CO_2 is taken to be the same as OH broadening by N_2. There is very limited data available for OH broadening by molecular hydrogen.[17] These results indicate a value of $2\gamma = 27.6 \times 10^{-5}$ cm^{-1} $Torr^{-1}$ which were obtained at room temperature. This value is however surprisingly high (it is almost the same as OH broadening by molecular nitrogen) and does not agree with the above argument, since H_2 is even smaller in size than the atomic He. For the present calculations, however, we will assume that the effect of H_2 as a broadener on OH can be neglected. Since for most practical purposes, in flame regions where the H_2 concentration is high the OH concentration would be low (unburned fuel) and therefore a small contribution to the overall absorption. Hence, the non-resonance broadening of OH induced by collisions with O_2, N_2, and CO_2 is given by

$$2\gamma_{NR} = P(296/T)^{0.59} [18.8\, X_{O2} + 28.5\, X_{N2} + 28.5\, X_{CO2}] \times 10^{-5} \text{ cm}^{-1} \qquad (20)$$

Where P is the total pressure (Torr), T is the temperature (K), and X is the mole fraction.

The line shape of OH transitions induced by collisions with water molecules is more complicated. This complication arises from the fact that the collision-induced broadening of OH by water molecules are due to near-resonant interaction of the two species. In this case, the broadening is strongly J-dependent. Since OH and water molecules have almost the same molecular weights, there would also be speed changing collisions that would modify the Doppler linewidth of the absorption transition (Dieke narrowing).[18] As a result, the OH line shape in environments where there exists a considerable amount of water vapor would be given by the collisional narrowing profile.

To compute the homogeneous broadening of OH due to collisions with water molecules, it may be assumed that the extent of this broadening depends on the population of water molecules in the rotational levels that are contributing to the near-resonance interaction between the two species. Due to the complicated spectra of water and the nature of the interaction there exists no analytical formula to compute this broadening. As a result, this broadening should be determined by an empirical formula. To arrive at this empirical formula, it is recognized that within the frame work of the impact approximation the broadening is given by Eqs. (17) and (19), where $U(R) = C_3/R^3$ for resonant interaction. Substituting for U(R) in Eq. (19) and computing Eq. (17), the full width at half maximum of Lorentzian linewidth is given by

$$\Delta\nu_R = 2\gamma_R = C' P T X_{H2O} \qquad (21)$$

where C' here is a coefficient that has to be determined from the available experimental data and based on the above argument should have a form as

$$C' = A \exp[-BE_{J''}/(k_B T)] \qquad (22)$$

where $E_{J''}$, k_B, and T have their usual definitions, and A and B are constants that must be determined from the experimental results. Since the homogeneous linewidth of OH induced by collisions with water molecules behave differently for low ($K'' \leq 2$) and high ($K'' > 2$) rotational levels,[14,18] the coefficient B will be determined separately for each case. To determine the

coefficient B the data obtained by Shirinzadeh, B.[18] is used. To do so, the value of log ($2\gamma_R$) for the OH transitions $R_2(3)$, $R_2(4)$, and $R_2(7)$ (Fig. 5.17 Ref. 18) have been plotted as a function of the energy of the rotational levels. Since the measurements were performed at a temperature of 1330 K, the slope of 7.833×10^{-4} determined from this plot results in a value of B = 0.72 for K" > 2. By considering 2/3 of water and 1/3 of O_2 in the cell a value of 3.92×10^{-4} is deduced for the coefficient A. Hence the equation determining the collision induced broadening of OH due to water molecules, where K" > 2, can be expressed as

$$\Delta\nu_R = P(1330/T)\, X_{H2O}\, 3.92 \times 10^{-4} \exp[-BE_{J''}/(k_B T)]\ \text{cm}^{-1};\ B = 0.72 \qquad (23)$$

For the $Q_1(4)$ transition of OH, Eq. (23) results in a $T^{-0.5}$ temperature dependence in good agreement with the dependence observed in ref. 14. For K" $\leq$ 2, the same value for the coefficient A is used. By considering the extent of broadening due to the $P_1(2)$ transition in Fig. 5.17 ref. 18 which is obtained for a temperature of 1330 K, a value of 0.48 is deduced for the B coefficient. Hence the equation describing the resonance broadening of OH for K" $\leq$ 2 is the same as Eq. (23) with a B = 0.48. For the $P_1(2)$ transition broadened by 10 Torr of water molecules at room temperature, the measured broadening is $\Delta\nu_R = 0.0142\ \text{cm}^{-1}$ (ref. 16) and the calculated value using the above prescription is $\Delta\nu_R = 0.0145\ \text{cm}^{-1}$.

The collision-induced narrowing parameter due to near-resonant interaction of OH with water molecules is computed in the same way described in ref. 18, i. e., $\alpha/(2\pi) = 2\gamma_R/(2\pi)$ is the narrowing parameter (see Eq. (15)). Finally, it is also noted that resonance interaction does not produce any collision-induced shift in the line center, and thus no shift needs to be considered in this case.

2.2. Fast fourier transform

In the previous section a description of the theory used to compute the tau-values for eight spectral channels and for a single spatial position was given. For simultaneous measurements of the tau-values at 10 spatial positions, a scheme of amplitude modulation (AM) of the light followed by transient digitization of the signal that contains all the AM frequencies is used. That is, a chopper wheel modulated the intensity of the light for each spatial position with a square waveform at a different frequency ranging from 1500 to 4200 Hz with an almost equal frequency spacings of 300 Hz. Fast fourier transform techniques were then utilized to discern the AM signals from each other. The rationale for this design was that the system must provide sufficient signal-to-noise ratio for detection (reduction in the dc background), must be small in size, and must be rugged and easy to operate. For example, if lock-in amplifiers were to be used for phase sensitive detection of these signals, 90 (9 spectral channels and 10 spatial positions) lock-in amplifiers would have been required. This would have made the system enormously large. In addition, lock-in amplifiers require reference signals with phase adjustment which would complicate the system even further. The FFT technique bypasses the above problems, but generates some new ones. The FFT requires a fast digitizer, the results are sensitive to the phase shifts (the same is true for lock-in amplifiers), aliasing is a problem, and finally a larger noise level is expected for a dc window (cross talk between near neighboring frequencies due to a truncated wave train). Here a procedure which increases the signal-to-noise ratio and decreases the cross talk between various AM frequencies will be given.

In the present experimental setup, the signal detected by a photomultiplier tube (PMT) as a function of time is given by

$$f(t) = \sum_{m} g_m(t) \tag{24}$$

where

$$g_m(t) = (2A_m/\pi) \sum_{n=1}^{\infty} \{-1/(2n)\,[(-)^n - 1] \sin(2\pi n\, \nu_m t + \Phi_m)\} \tag{25}$$

is the ac component of a square wave having an amplitude A_m, a frequency ν_m, and a phase Φ_m. It is seen here that only the odd harmonics are present. This makes it possible to choose the fundamental frequencies, ν_m, such that the third harmonic of the smallest frequency is larger than the first harmonic of the largest frequency. In this system, the AM frequencies ν_m cover a range from 1500 to 4200 Hz with almost equal frequency spacing of 300 Hz to satisfy the above requirement.

It is known that discrete sampling of a periodic wave train can result in aliasing effect, i. e., higher harmonics can be spuriously moved into the frequency range of interest and thus generate noise. To minimize this effect, the above signal is processed by a 5 kHz, six-pole Bessel filter before it is digitized and stored in the computer. Hence, Eq. (25) can be simplified to

$$g_m(t) = (2A_m/\pi) \sin(2\pi\, \nu_m t + \Phi_m) \tag{26}$$

A minimum sampling frequency of 10 kHz (time between samples = Δt = 100 microseconds) was used to digitize the waveform (digitizer is capable of achieving 50 kHz sampling rate). When 50 kHz data acquisition rate was used, the data was broken into 10 kHz data sets before the discrete fast fourier transform operation was performed. The discrete waveform, f_j, can be obtained by replacing t with $j\Delta t$ in Eq. (26). For fast fourier transform, the number of data points selected should be a multiple of 2, i.e., $K = 2^N$, where N is an integer. This means that j assumes values of 0, 1, 2, ..., K - 1.

To minimize cross talk and noise ("leakage") from the neighboring frequencies, the Hanning window is utilized. The Hanning window, w_j, is defined as

$$w_j = (1/2)\{1 - \cos[2\pi\, j/(K - 1)]\} \tag{27}$$

and the FFT is performed on the product, $f_j\, w_j$. The discrete fourier transform thus obtained is corrected for amplitude using a procedure described in Ref. 19. This correction minimizes the error associated with the discreteness of the FFT results, since the peak for a given frequency may lie between two bins.

To obtain the tau-values, data is taken with and without any OH present in the sample volume. These results are then stored in the computer separately. The FFT is then performed on these results. To reduce random noise, the FFT was performed on sections of data each containing 2^{10} points. The tau-values are then computed for each section separately and are averaged to reduce the random noise to a level of <1%. As it is seen in Eq. (26), the FFT amplitudes depend on the phase Φ_m. Therefore, it is very important to keep this phase the same between Flame on and off condition. This was done by installing a separate hole on the chopper wheel. On one side of the wheel an LED is installed and on the other side a detector (photodiode) is placed. The detector output is a square pulse for every revolution of the wheel. This signal is then compared

with the internal clock pulses of the digitizer. When a correlation within 1 microsecond between the two pulses occur a trigger pulse is generated. This pulse starts the data acquisition sequence. This insures that the phase remains the same between the Flame on and off condition. The chopper wheel speed is monitored and remains constant during the data acquisition session.

3. EXPERIMENTAL

Fig. 1 shows a schematic diagram of the 10-position OH instrument. The system consists of three parts, namely, a source, a receiver, and a data acquisition (fast digitizer plus a computer) unit. It is seen in this figure, that the light from the source unit is brought to the sample volume via ten 400 micrometer fibers. The light, after a traversal path through the sample volume, is collected by another ten fibers (the same diameter) and is detected by the receiver unit. The signal from the receiver unit is then digitized by a fast digitizer capable of 20 seconds of simultaneous data acquisition on 11 channels at a rate of 50 kHz. This transient data is then transferred to a computer for data analysis and storage.

3.1. The source unit

Figure 2 depicts a schematic diagram of the source unit. This unit includes a dc mercury lamp, a low pressure (1 Torr) water-vapor microwave discharge lamp, and a chopper wheel. It also includes the OH and the mercury lamp intensity monitoring systems. The OH emission spectra generated by the water-vapor microwave discharge lamp is collected by a 12-probe fiber bundle with each fiber measuring 400 micrometers in diameter. Ten of these fibers are then brought to a chopper wheel where the light in each fiber is amplitude modulated with a square waveform at a different frequency (see section 2.2 for description). At the same time, the light from the mercury lamp is collected, processed by an interference filter, and imaged on the same bundle. This interference filter has a bandwidth of 10 nm and a peak transmission of 70% which is centered on mercury emission lines near 365 nm. This is to reject the mercury lines at 313.17 and 312.57 nm which overlap the OH spectra. The reason for the presence of mercury light near 365 nm is to insure that the absorption that takes place in the sample volume is due to OH and not due to blockage or deflection of the light. For this reason, this channel in the data acquisition is called the path attenuation channel. To minimize the effect of variations in the intensities of the mercury and the OH lamps on the detected signals, these intensities are monitored by two detectors. To monitor the OH lamp intensity the light in one of the 12-fiber collection bundle is brought to a detector. This detector consists of an interference filter with a bandwidth of 10 nm that is centered at 310 nm, and a photodiode detector equipped with current-to-voltage amplifier. To monitor the mercury light intensity, the detector consists of an interference filter with a bandwidth of 10 nm that is centered at 365 nm, and a photodiode detector with a current-to-voltage amplifier. The two lamp monitoring signals are digitized on two separate channels in the digitizer.

3.2. The receiver unit

After a traversal path through the sample volume the light is collected by the catch fibers for 10 positions and is brought to the receiver unit (Fig. 1). Inside the receiver unit (Fig. 3) the 10 fibers are connected to a fiber array bundle measuring 4.7 mm in height which is placed at the entrance slit (200 micrometer in width and 2 cm in height) of a spectrograph. The 1/4 m spectrograph is equipped with a 2400 grooves/mm classical grating blazed at 300 nm and has a dispersion of 2 nm/mm. At the exit plane of the spectrograph there exists a two dimensional fiber array bundle measuring 7.5 mm in height and 6 mm in width. As it is seen in Fig. 3, the exit plane fiber bundle array provides 8 spectral channels for OH detection. Fig. 4 shows the diameters of the fiber arrays for each spectral channel and the OH transitions that they cover. This figure is obtained by computing the OH spectra using the dispersion of the spectrograph mentioned above and adjusting the grating such that the 313.17 nm mercury line is centered on channel 6 (200 micrometer in diameter) fiber array. It should be noted that the actual transmission

for each spectral channel does not behave like a square top profile and Fig. 4 is for illustration purposes only. In addition to the 8 spectral channels for OH, there also exists a path attenuation fiber array bundle for the detection of the 365 nm mercury line. This fiber array has the same height as the OH fiber arrays and is made of fibers with a diameter of 600 micrometers. The light from each column of fibers is then detected by a photomultiplier tube (PMT). There are eight PMTs for OH spectral channels and one for the path attenuation channel. The signal from each PMT after the current-to-voltage amplification is digitized and stored in the computer.

3.3. The data acquisition system

The data acquisition system consists of a fast digitizer and a computer. The digitizer is capable of acquiring data at a rate of 50 kHz on eleven channels simultaneously for a period of 20 seconds. It is equipped with a 5 kHz bandpass, six-pole, Bessel filter on the input. This is to minimize the aliasing on the FFT results. An external trigger described in the section 2.2 starts the data acquisition session. After the data acquisition is completed on the digitizer, the data is transferred to the computer for permanent storage and analysis.

4. RESULTS AND DISCUSSIONS

4.1. OH resonance microwave discharge lamp

The characterization of the emission spectra of OH in the low pressure water vapor microwave discharge lamp plays an important role in the design of this instrument. The parameters of interest are the translational temperature of OH and the peak intensities of the OH emission spectra as a function of the microwave power and the pressure in the discharge cell. The translational temperature was determined by tuning the frequency of an intra-cavity frequency-doubled, single-frequency, tunable cw ring dye laser across isolated OH transitions and obtaining the absorption profile of OH. These absorption profiles were then fit to a Gaussian profile and thus the translational temperature of OH in the discharge cell were deduced from the observed linewidth. The peak intensities of the OH emission spectra in the discharge cell were measured using a 2 meters monochromator with a 2160 grooves/mm grating blazed at 500 nm. With input and output slit widths of 10 micrometers, an spectral resolution of .0047 nm was obtained. This spectral resolution was verified using the mercury line-doublets near 313.17 nm and was sufficient to resolve the majority of the OH spectral lines. The measured spectra was then fit using the computed spectra of OH derived from the rotational energy terms tabulated in Dieke and Crosswhite.[9] In this way, the peak emission intensities of 220 lines in the $^2\Sigma^+(v'' = 0)$ to $^2\Pi(v' = 0)$ and $^2\Sigma^+(v'' = 1)$ to $^2\Pi$ $(v' = 1)$ rotational electronic transitions of OH were measured and stored in the computer. The variations of this spectra with the microwave power (constant pressure of 1 Torr) was also studied and the results indicated that, the relative intensities remained the same as the microwave power was varied. The variation with pressure at constant microwave power, however, indicated that the relative intensities would change with cell pressure. Specifically, it was observed that the addition of the Ar buffer gas to the cell (up to 10 Torr of total pressure) shifted the intensity distribution more toward the (0-0) band of OH. To maximize the emission intensity and to operate the microwave discharge at a temperature not too high, the OH instrument was operated at a cell pressure of 1 Torr of water vapor and a microwave power of 70 watts. At this microwave power the translational temperature of OH was measured to be 720 K.

4.2. Determination of the transmission profiles of the exit plane fiber bundle

To compute the transmission, Tau_i, for each spectral channel, it is necessary to measure the transmission profile, $T_i(v)$, of the exit plane fiber bundle for every spatial position (see Eq. 1). These measurements were performed after all the alignment and optimizations of the signals were

completed and the input and the output fiber bundles were locked in place. The measurements were performed in two steps: first the relative line shape of each spectral channel for every spatial position was measured, and second the absolute frequency calibrations for these transmission profiles were determined.

To determine the relative line shape for each spectral channel and for every spatial position, a dc mercury lamp was used as the light source. The light from the mercury lamp was collected by a fiber corresponding to a given spatial position and was directed to the input slit of the spectrograph. The spectrograph was then scanned and the intensity profile of the mercury line near 296.73 nm across each spectral channel was recorded. (The detection system was the same as in the case of OH measurements.) Since these spectra was obtained as a function of time, in order to convert it to frequency, mercury lines 296.73, 302.15, 312.57, and 313.17 nm were scanned across spectral channel 6 (200 micrometer fiber array) at the same speed as the above scans. In this way, a plot of the time versus frequency was obtained.

To set the spectrograph for OH measurements, the mercury line 313.17 nm was peaked on spectral channel 6 and for spatial position 5. Therefore, it is important to know the relative shift of this line with respect to other spatial positions. To do so, the light in position 5 was chopped at a frequency of 2068 Hz and the light in the other positions (one at a time) was chopped at a frequency of 2482 Hz. The two signals thus generated underwent phase sensitive detection by two lock-in amplifiers. Care was taken to insure that there is no shift between the two lock-ins when the same signal was applied to both. The spectrograph was then scanned at the same rate as before and the mercury line 296.73 nm was detected on spectral channel 6 for both positions, simultaneously. In this way, the relative shift in spectral channel 6 between the spatial position 5 and every other position was determined. By combining the above data, the transmission profiles in time for 8 spectral channels and 10 spatial positions were converted to the absolute frequency units. Fig. 5 depicts the transmission profile for 8 spectral channels and for the spatial position 5 as a function of the frequency (cm^{-1}). The variation in the amplitudes reflect the transmission of the bundles and the gain differences between the photomultiplier tubes. It is also seen here that the 8 spectral channels cover a frequency range from ~ 32700 to 31400 cm^{-1}. These transmission profiles are used in the computation of the tau-values using Eq. (1).

4.3. Numerical fast fourier transform (FFT) results and deduced tau-values

Fig. 6 shows a plot of a typical numerical FFT result. The procedure is described in the theory section 2.2. It is obtained for the spectral channel 4. In this figure, the FFT is performed on the transient data which was taken at a rate of 10 KHz (100 microseconds between points in the time domain), and a total number of 1024 points. As seen here, the chopping frequencies are well separated and the third harmonic of the smallest chopping frequency lies beyond the first harmonic of the largest chopping frequency. Also there is no detectable second harmonics present in this figure. The cross talk between the chopping frequencies is negligible. To deduce the tau-values, the transient data was divided into one hundred 1024 data point sections. Each section was then normalized to the corresponding section in channel 9 (path attenuation channel). The ratio of each section between the Flame on and off condition results in the tau-value for that section. Averaging 100 of these sections results in a tau-value which is used to deduce OH concentration times the path length, and the rotational temperature of OH in the combustion environment. When comparing two OH off conditions (tau = 1), a typical uncertainty of about 1% or less is obtained and the deduced tau-values are equal to 1 within this uncertainty.

4.4. OH absorption results obtained on a methane-air flat flame burner
(*testing of the apparatus*)

To test the 10-position OH apparatus, a Methane/Air "flat" flame burner with a nitrogen shroud gas was used. In these experiments the fuel-to-air ratio was adjusted to one. Measurements were

performed at a height of 5 mm above the burner surface. Two sets of absorption measurements were performed: one was with the dye laser system, and the other was with the 10-position OH instrument. In both cases, the beam geometries were identical. The only difference was that for the experiments using the dye laser the beam made a round trip traversal through the sample volume (flame), while for the OH apparatus only a single-path absorption measurements were made.

Fig. 7 shows a typical absorption profile of OH obtained with the dye laser system. It is obtained for the $R_2(7)$ transition of OH near 307 nm. The points are the data and the line represents the best fit to the data using the hard collisional narrowing profile. The product of the density of OH times the path length deduced from this figure is $(2.55 \pm 0.25) \times 10^{16}$ molecules/cm^2. This [OH].L is determined using the area under the profile, and the rotational temperature of OH deduce from measuring this area for a number of rotational electronic transitions. Fig. 8 shows a semi-log plot of the relative population of OH as a function of the energy of the rotational levels. The effective rotational temperature of OH deduced from this plot is 1619 ± 24 K.

For measurements performed with the OH apparatus, to deduce the OH concentration times the path length and the rotational temperature of OH from the measured tau values, it is necessary to form a library of the computed tau-values under these experimental conditions. Constant input parameters for these computations are total pressure (P = 760 Torr), and the mole fraction of molecular nitrogen ($X_{N2} = .78$), oxygen ($X_{O2} = .04$), and water ($X_{H2O} = .18$). Variable input parameters are the temperature and the [OH].L. The temperature was varied from 500 K to 2200 K in 50 K intervals. The [OH].L was varied geometrically from 10^{15} to 10^{19} molecules/cm^2 with a step of $10^{.025}$, i. e., [OH].L = $10^{15} \times 10^{(i \times 0.025)}$; where i = 0, ..., 160. In this way a tau library for 10 positions, 35 temperatures, and 161 [OH].L was generated. Figs. 9, 10, and 11 show plots of the computed tau-values for the spatial position 5 as a function of the temperature at three values of the [OH].L. Also for the sake of easy reference, at the bottom of each figure, the computed tau-values for the temperatures of 1400 K and 1700 K are listed for 8 spectral channels. It is seen from these plots that in order to make accurate determination of the rotational temperature of OH, measurements of the tau-values would have to be made with an uncertainty of less than 1%. It is also seen that in the temperature range from 1400 K to 1700 K, the range of the [OH].L that may be considered is from 10^{16} to 10^{18} molecules/cm^2. For the measurements performed on the flat flame burner using this instrument, a single-path absorption was used. Based on the dye laser results, this would translate to an [OH].L of $(2.55 \pm 0.25) \times 10^{16}$ molecules/cm^2. This is in the acceptable range for this instrument. Many measurements were performed using this instrument on the flat flame burner. In fact nine fibers were brought into a ring configuration at the same height around the circular burner and simultaneous measurements on the nine positions were performed. One fiber was located exactly where the dye laser beam was located. The data obtained were then fit using a non-linear least squares fitting routine to the computed tau library. The [OH].L and the rotational temperature of OH were deduced. Results indicated different [OH].L and rotational temperatures for different axial positions around the burner. At first, it was thought that these differences were due to some systematic error in the instrument. However, when fibers were interchanged, the results stayed the same, which was an indication that the instrument was working properly and that the differences were actually due to the non-uniformities present in the flat flame burner. Measurements performed at the same position as the dye laser measurements resulted in an [OH].L of $(2.3 \pm 0.2) \times 10^{16}$ molecules/cm^2 and a rotational temperature of (1550 ± 100) K over a data acquisition time of 2 seconds which is in good agreement with the above dye laser results.

5. CONCLUSIONS

An OH line-of-sight absorption measurement system, capable of obtaining [OH].L and the rotational temperature of OH simultaneously at 10 spatial positions, has been demonstrated. The instrument is rugged and can be used in cw, harsh wind tunnel and engine environments, where

optical access, vibrations, and lack of expert personnel to operate the apparatus becomes a road block. Presently, with a data acquisition rate of 50 KHz, the system can measure rotational temperature and OH concentration every 2 seconds. This time, however, can be reduced by increasing the efficiency of the light gathering fibers or by increasing the data acquisition rate. This instrument is scheduled to be tested in a hypersonic scramjet facility in the near future.

6. ACKNOWLEDGEMENTS

The authors thank Dr. R. J. Exton for his interest and a number of helpful discussions through the course of this project.

7. REFERENCES

1. P. Ewart and M. Kaczmarek, "Two-dimensional mapping of temperature in a flame by degenerate four-wave mixing in OH," Appl. Opt. 30, PP. 3996-3999, 1991.

2. B. Yip, P. M. Danehy, and R. K. Hanson, "Degenerate four-wave mixing temperature measurements in a flame," Opt. Lett. 17, PP. 751-753, 1992.

3. K. J. Rensberger, J. B. Jeffries, R. A. Copeland, K. Kohse-Hoinghaus, M. L. Wise, and D. R. Crosley, "Laser-induced fluorescence determination of temperature in low pressure flames," Appl. Opt. 28, PP. 3556-3566, 1989.

4. P. H. Paul, U. E. Meier, and R. K. Hanson, "Single-shot, multiple-camera planar laser-induced fluorescence imaging in gaseous flows," AIAA-91-0459, 1991.

5. E. W. Kaiser, K. Marko, D. Klick, L. Rimai, C. C. Wang, B. Shirinzadeh, and D. Zhou, "Measurement of OH density profiles in atmospheric-pressure propane-air flames," Combust. Sci. and Tech. 50, PP. 163-183, 1986.

6. D. F. Davidson, A. Y. Chang, M. D. DiRosa, and R. K. Hanson, "Continuous wave laser absorption techniques for gasdynamic measurements in supersonic flows," Appl. Opt. 30, PP. 2598-2608, 1991.

7. W. R. Lempert, "Microwave resonance lamp absorption technique for measuring temperature and OH number density in combustion environments," Combus. and Flames 73, PP. 89-98, 1988.

8. G. B. Northam, W. A. Lempert, G. S. Diskin, Ray Gregory, and R. A. Bell, "Supersonic combustion performance of hydrogen/hydrocarbon mixtures as determined by a nonintrusive temperature monitor," AIAA-88-3293, 1988.

9. G. H. Dieke, and H. M. Crosswhite, "The ultraviolet bands of OH," J. Quant. Spectrosc. Radiat. Transfer. 2, PP. 97-199, 1962.

10. C. C. Wang, and C. M. Huang, "Accurate determination of the band oscillator strength for the (0,0) ultraviolet transitions of OH," Phys. Rev. A21, PP. 1235-1236, 1980.

11. P. L. Varghese, and R. K. Hanson, "Collisional narrowing effects on spectral line shapes measured at high resolution," Appl. Opt. 23, PP. 2376-2385, 1984.

12. A. K. Hui, B. H. Armstrong, and A. A. Wray, "Rapid computation of the Voigt and complex error functions," J. Quant. Spectrosc. Radiat. Transfer 19, PP. 509-516, 1978.

13. A. Corney, "Atomic & laser spectroscopy," Clarendon Press, Oxford, PP. 228-270, 1977.

14. C. C. Wang, D. K. Killinger, and C. M. Huang, "Rotational dependence in the linewidth of the ultraviolet transitions of OH," Phys. Rev. A22, PP. 188-191, 1980.

15. E. C. Rea, Jr., A. Y. Chang, and R. K. Hanson, "Collisional broadening of the $A^2\Sigma^+ <---X^2\Pi(0,0)$ band of OH by H_2O and CO_2 in atmospheric-pressure flames," J. Quant. Spectrosc. Radiat. Transfer 41, PP. 29-42, 1989.

16. B. Shirinzadeh, D. M. Bakalyar, and C. C. Wang, "Measurements of collision-induced shift and broadening of the ultraviolet transitions of OH," J. Chem. Phys. 82, PP. 2877-2879, 1985.

17. R. Engleman, Jr., "Collision broadening of transient absorption spectra: I. hydroxyl linewidth in the (0,0) (A<---X) transition at low temperatures," J. Quant. Spectrosc. Radiat. Transfer 9, PP. 391-400, 1969.

18. B. Shirinzadeh, "Absorption lineshape and laser-induced fluorescence measurements of OH," Ph. D. thesis, University of Michigan, PP. 62-94, 1988.

19. J. C. Burgess, "On digital spectrum analysis of periodic signals," J. Acoust. Soc. Am. 58, PP. 556-567, 1975.

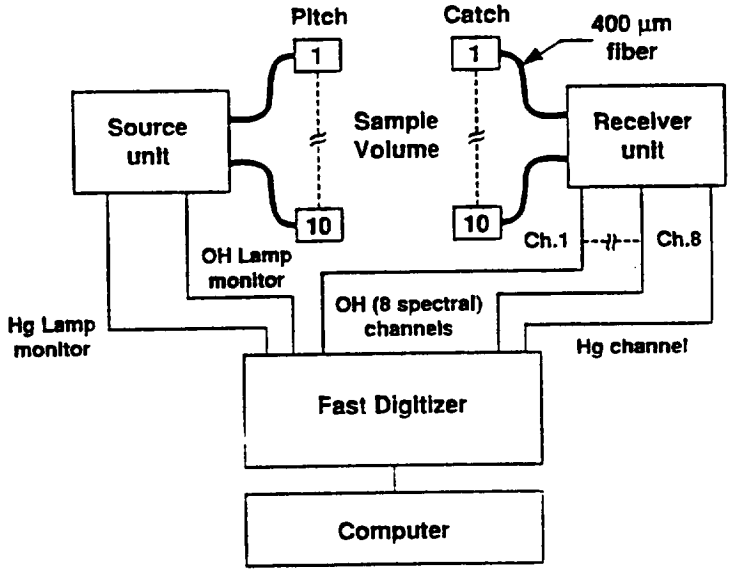

Fig. 1. Schematic diagram of the 10-position OH instrument.

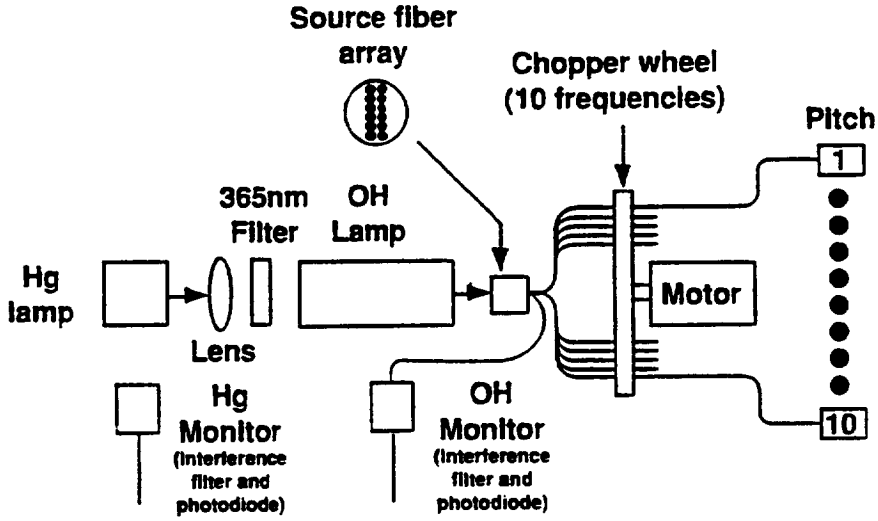

Fig. 2. Schematic diagram of the source unit.

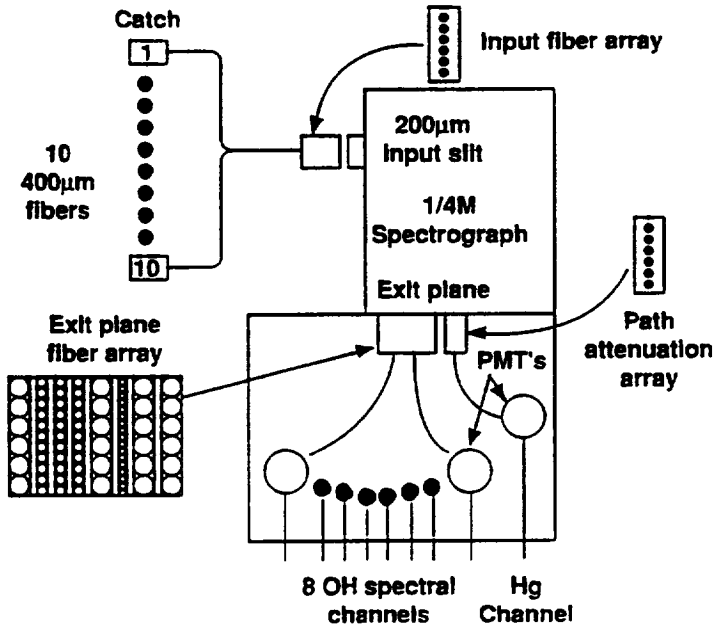

Fig. 3. Schematic diagram of the receiver unit.

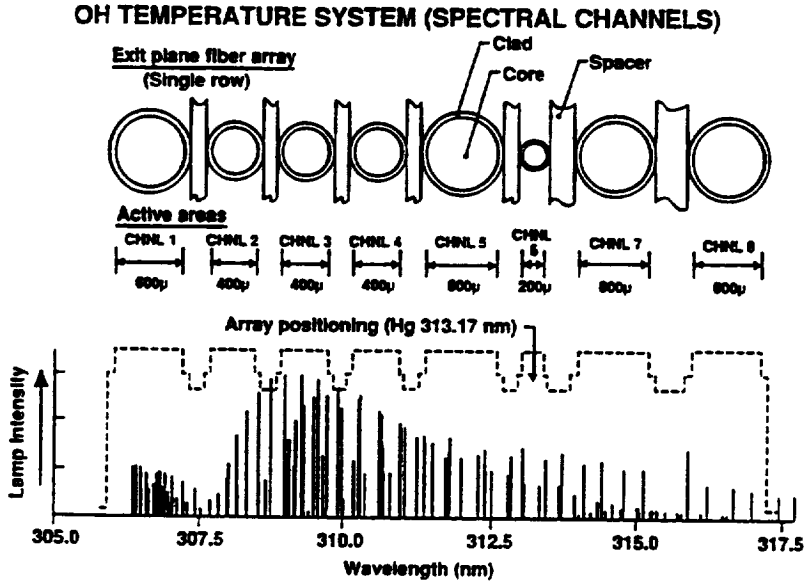

Fig. 4. Schematic diagram of the exit-plane fiber array bundle. The OH spectrum is shown for easy reference. See text for detail.

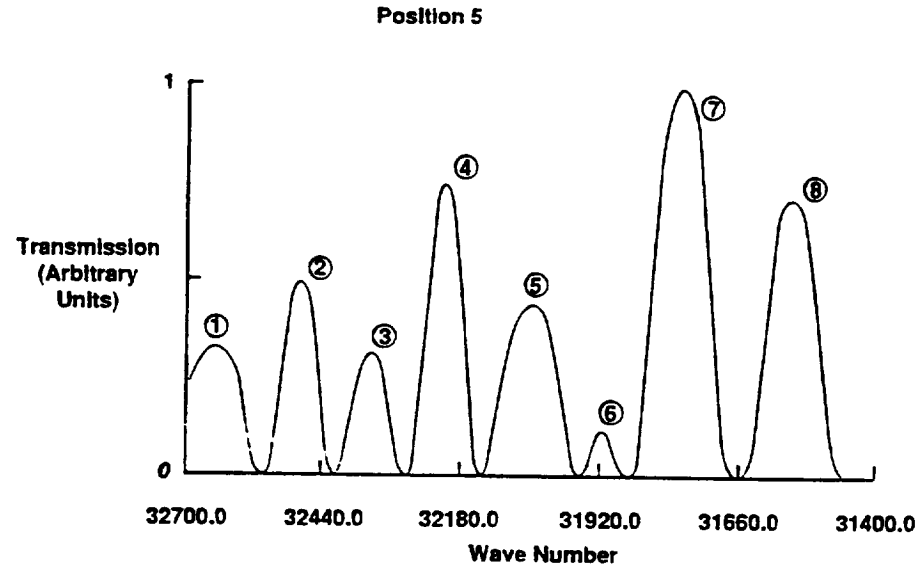

Fig. 5. A plot of the measured transmission (T(ν)) profile of the exit-plane fiber array bundle for position 5 as a function of the frequency (cm^{-1}).

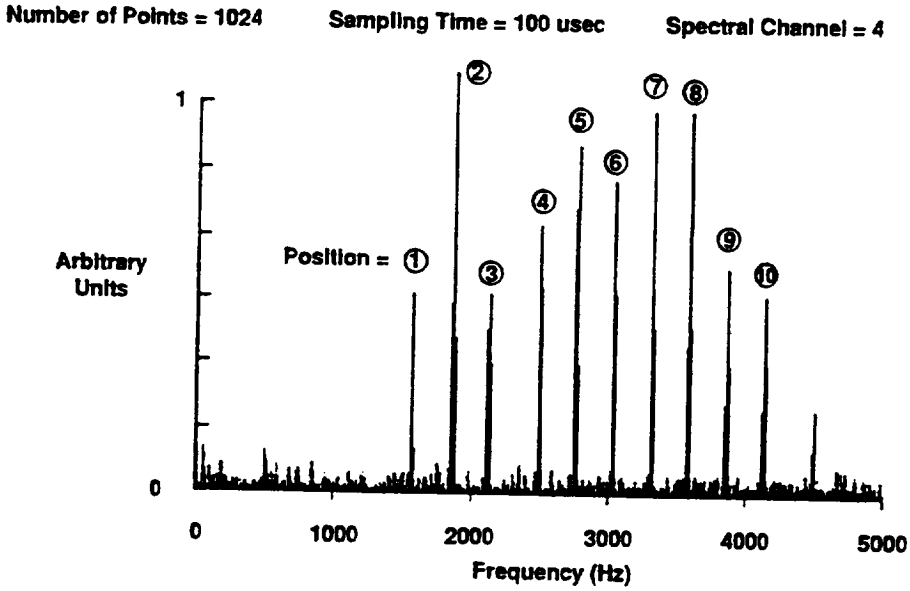

Fig. 6. Plot of a typical FFT spectrum obtained for the spectral channel 4.

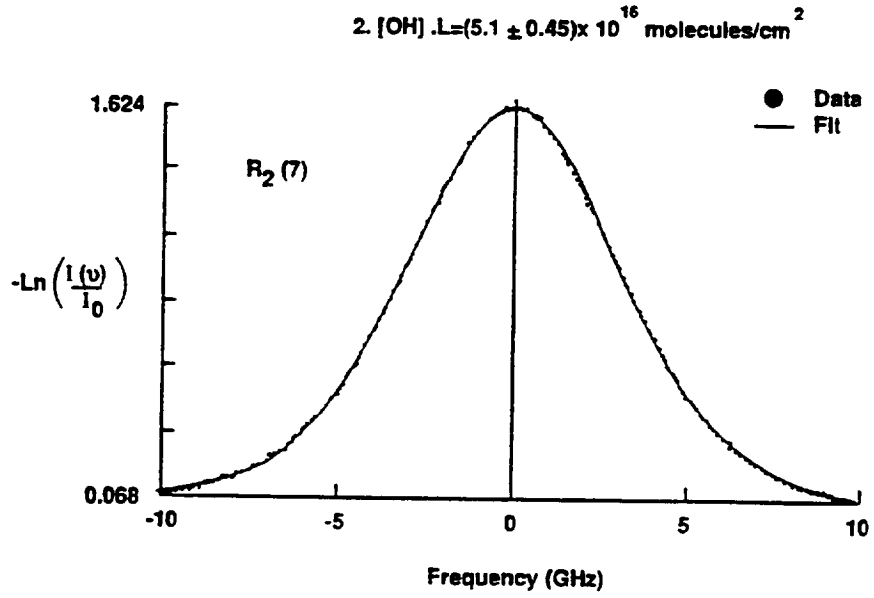

Fig. 7. Plot of a typical absorption profile of OH obtained in the flame using the dye laser system as function of the frequency detuning from the line center. The points are the data and the line represents the fit to the data. See text for detail.

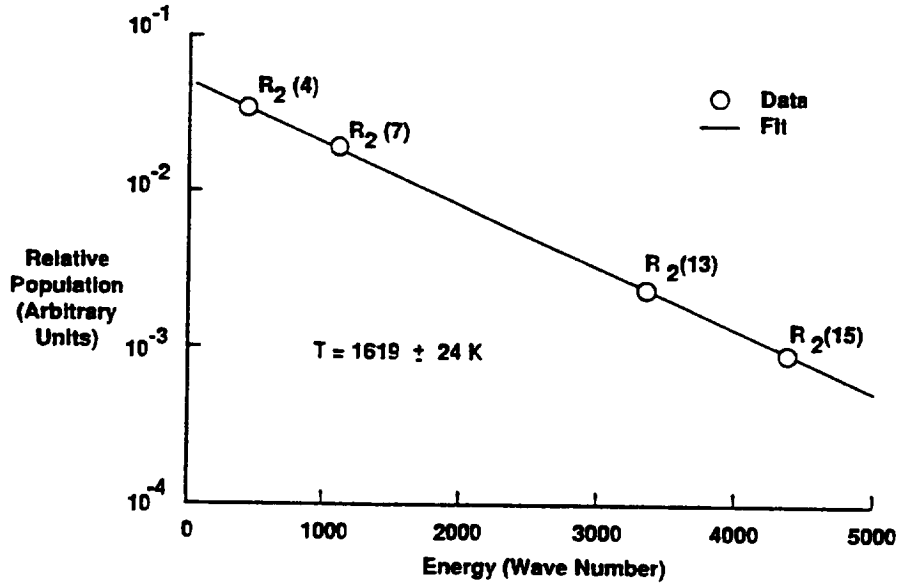

Fig. 8. A plot of the measured relative population of OH as a function of the energy of the rotational levels. The line represents the least squares fit to the data. Data is obtained using the dye laser system and the flat flame burner. See text for detail.

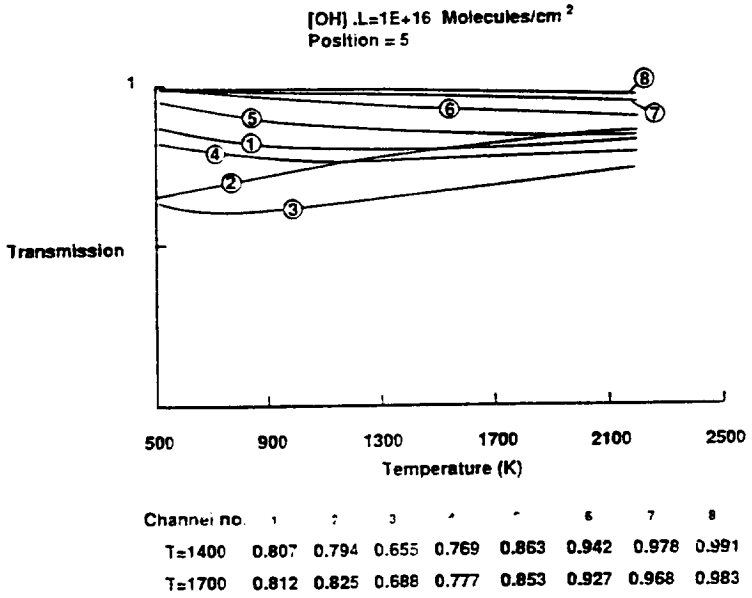

Channel no.	1	2	3	4	5	6	7	8
T=1400	0.807	0.794	0.655	0.769	0.863	0.942	0.978	0.991
T=1700	0.812	0.825	0.688	0.777	0.853	0.927	0.968	0.983

Fig. 9. A plot of the computed transmission (tau-value) profiles obtained with a product of the OH concentration times the path length of 10^{16} molecules/cm^2 as a function of the temperature for eight spectral channels. The computations have been performed for spatial position 5. The number next to each curve denotes spectral channel. See text for detail.

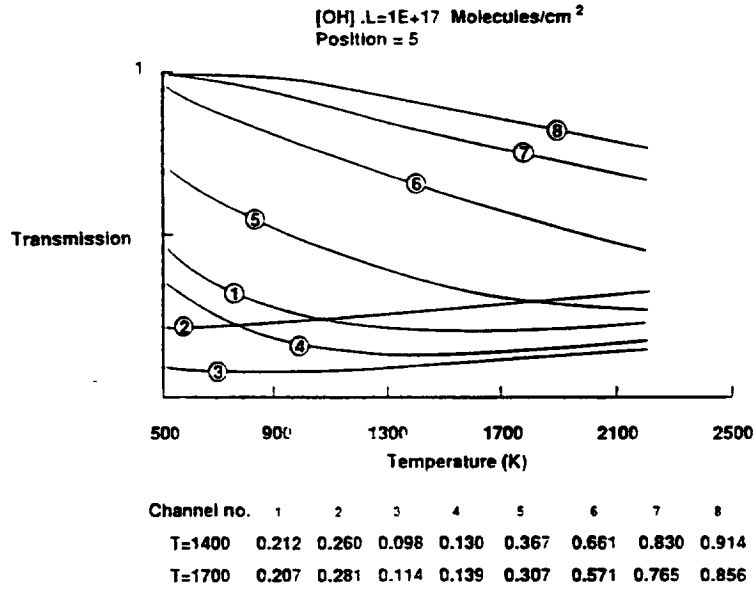

Channel no.	1	2	3	4	5	6	7	8
T=1400	0.212	0.260	0.098	0.130	0.367	0.661	0.830	0.914
T=1700	0.207	0.281	0.114	0.139	0.307	0.571	0.765	0.856

Fig. 10. The same as Fig. 9, except that the [OH].L is now 10^{17} molecules/cm^2.

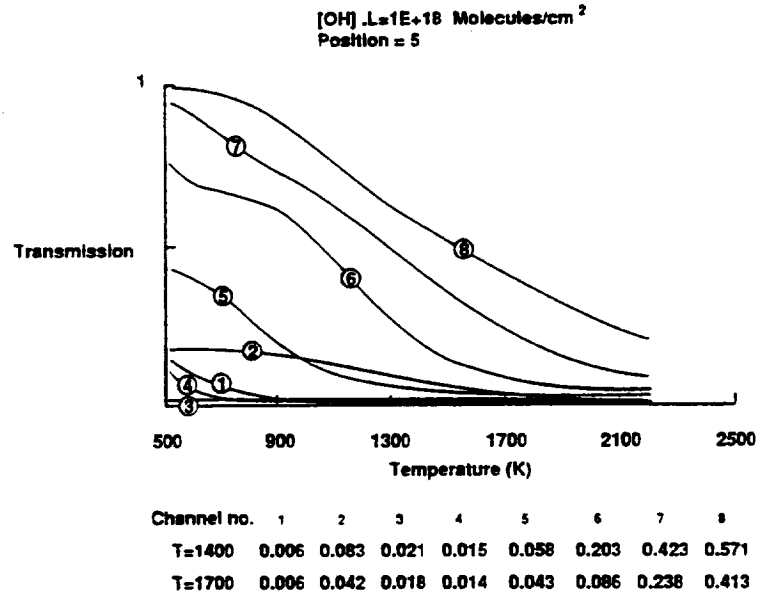

Channel no.	1	2	3	4	5	6	7	8
T=1400	0.006	0.083	0.021	0.015	0.058	0.203	0.423	0.571
T=1700	0.006	0.042	0.018	0.014	0.043	0.086	0.238	0.413

Fig. 11. The same as Fig. 9, except that the [OH].L is now 10^{18} molecules/cm^2.